http://journal.uir.ac.id/index.php/JGEET

E-ISSN : 2541-5794
P-ISSN : 2503-216X

Journal of Geoscience,
Engineering, Environment, and Technology
Vol 10 No 04-2/2025

RESEARCH ARTICLE

4D Seismic Analysis of Hydrocarbon Reservoir at Hugin Formation, Volve Field, North Sea

Yasinta Farania Agustin [1], Muhammad Husni Mubarak Lubis [1,*]

[1] Department of Geophysical Engineering, Faculty of Technology Exploration and Production, Universitas Pertamina, Jakarta, 12220, Indonesia

* Corresponding author : muhammad.hml@universitaspertamina.ac.id
Tel.: +62 812-2256-8918
Received: Jul 31, 2025; Accepted: Jan 9, 2026
DOI: 10.25299/jgeet.2025.10.1.1.24368

Abstract

This study investigates the 4D seismic analysis of oil-filled hydrocarbon reservoirs in the Volve Field. A primary objective is to model reservoir changes resulting from water injection activities using a time-lapse model-based inversion approach. The study employs Volve 3D seismic data from 2002 as a baseline and 2010 data as a monitor. Well logs used for the inversion include injection wells F-4 and F-5 and production well F-12. Inversion of the baseline and monitor seismic volumes reveals a distribution of acoustic impedance values ranging from 6770 to 12008 (m/s)*(g/cc). Time-lapse analysis, conducted by differencing the inverted baseline and monitor acoustic impedance volumes, reveals an average increase of approximately 2.74% in acoustic impedance in the vicinity of the injection and production wells. This increase is interpreted as a response to the migration of injected fluids into the reservoir. The spatial distribution of impedance changes suggests that the injected fluids preferentially migrate within the Middle Zone, rather than the Lower Hugin Zone. This behavior is likely controlled by the increased shale content in the Lower Hugin Zone, which acts as a permeability barrier and restricts downward fluid movement.

Keywords: 4D Seismic Inversion, Acoustic Impedance, Time-lapse, Water Injection

1. Introduction

Reservoir pressure declines as hydrocarbon is produced. One approach to improve hydrocarbon production in fields experiencing declines is by injecting fluids, as demonstrated in the Volve Field, Norway. This study aims to enhance understanding of the behavior of the oil reservoir in the Hugin Formation over time. The Volve Field is one of Norway's significant oil-producing sites, with the Hugin Formation yielding peak production of up to 56,000 BOPD. However, since its discovery in 1993 and production started in 2008, this field has faced challenges in maintaining steady output. To address this, water injections have been implemented to sustain production levels. Monitoring reservoir conditions is also crucial to track injection fluid distribution and residual hydrocarbons for sustainable production. This study employs a time-lapse model-based inversion approach to model changes in the reservoir due to water injection. Using time-lapse seismic data, this study aims to reveal hydrocarbon distribution over time and to refine water injection strategies, optimizing production efficiency and sustainability.

2. Study Area

The study area is the Volve Field, part of the North Sea epicontinental basin in Norway. This oil-producing field has a reservoir interval at depths between 2750 and 3120 meters TVDSS, with thicknesses varying from 20 to 100 meters. Located in Block 15/9, about 200 kilometers west of Stavanger, Volve Field lies at the southern end of Norway's sector of the North Sea. Production began in 2008, reaching a peak output of 56,000 barrels of oil per day before the operations ceased in 2016 (Sen & Ganguli, 2019). The reservoir comprises Middle Jurassic sandstone in the Hugin Formation, structured as a small dome created by the collapse of nearby salt mountains during the Jurassic period (Szydlik et al., 2007). The dominant structural feature of Volve Field is a fault system formed by salt tectonics, with regional extension influences seen primarily in the western part. Production in this field is supported by water injections to maintain reservoir pressure. This injection process began in 2008 at a rate of approximately 7500 m^3/day, stabilizing to around 5000 m^3/day since 2012 (Sen & Ganguli, 2019). Specific wells, including injection wells F-4, F-5, and F-9, are dedicated to supporting production through this method. Stratigraphic column of The North Sea (**Figure 1**), where the main reservoir of this study was formed in the Jurassic period.

The Jurassic section of this field stratigraphy consists of shale lithology marked by high gamma rays. Hugin Formation is dominated by shallow marine sandstone. In addition, in the Sleipner Formation, there are also sandstone, coal, and shale lithologies.

Sastra et al. (2023) subdivided the Hugin Formation into three stratigraphic zones based on variations in formation depth. Their study demonstrates that these zones exhibit distinct petrophysical characteristics, including systematic variations in porosity, permeability, and water saturation, reflecting differences in reservoir quality and fluid distribution across the formation. Furthermore, the authors reported the differences in the average Vshale values among the three zones. The Middle Hugin zone is characterized by the lowest average Vshale, suggesting

relatively cleaner sandstone with better reservoir quality, whereas the Lower Hugin zone exhibits the highest Vshale, indicating increased shale content and potentially reduced reservoir performance. These vertical heterogeneities highlight the importance of zonation in accurately characterizing the reservoir properties.

In general, the rock properties in the reservoir are very good, with an average porosity of 21% and permeability varying from 100 mD to more than 10 D (Sen & Ganguli, 2019).

3. Data and Method

3.1 Seismic Data

This study uses 3D seismic data from 2002 as a baseline and 2010 as monitoring. The baseline data was acquired prior to the water injection process, while the monitor data was acquired two years after the injection was initiated. The data has been reprocessed for time-lapse analysis purposes in 2012. Both the baseline and monitoring seismic data have normal SEG polarity and a sample rate of 4 ms.

3.2 Well Data

This study utilizes data from three wells for inversion and analysis: injection wells F-4 and F-5 and production well F-12. Injection wells in the Volve Field are essential for maintaining reservoir pressure through water injections, thereby optimizing production in the production wells. Wells F-4 and F-5, specifically, play a critical role in the water injection program in this field. Water injection began at a rate of approximately 7,500 m^3/day per well, stabilizing at around 5,000 m^3/day since 2012. The primary objective of water injection is to enhance the hydrocarbon recovery factor, which represents the percentage of hydrocarbons extracted from the reservoir. By sustaining reservoir pressure, water injections facilitate the movement of hydrocarbons toward active production wells.

3.3 Normalized Root Mean Square (NRMS)

The Normalized Root Mean Square (NRMS) difference is a metric used to assess the differences between two seismic data volumes acquired at different times. This value is calculated using the RMS difference between the monitor data and the baseline dataset amplitude. Several factors can contribute to high NRMS values or poor repeatability between baseline and monitoring seismic data. These include variations in acquisition geometry (such as source and receiver positions), differences in data processing parameters, phase shifting, and other issues that may introduce noise into the data. In this study, the NRMS value categories proposed by Lumley (1996) are used as a guideline for implementing cross-equalization, as shown in **Table 1**.

Figure 2 indicates that the average value of the NRMS difference slice data at the top of the reservoir is 0.245. According to Lumley's (1996) categories, this baseline and monitor data exhibit 'very good repeatability,' allowing further processing to proceed without the need for cross-equalization. This NRMS evaluation was conducted within the 2200–2300 ms zone (or above the reservoir zone).

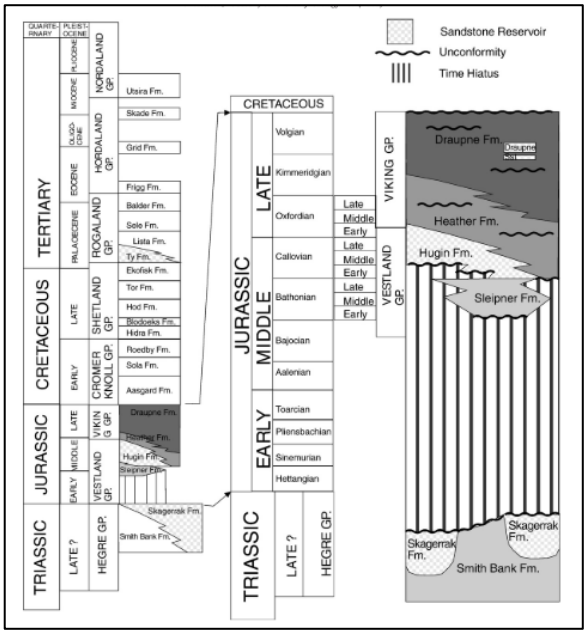

Fig. 1. Stratigraphic Column of the North Sea (Folkestad, 2008)

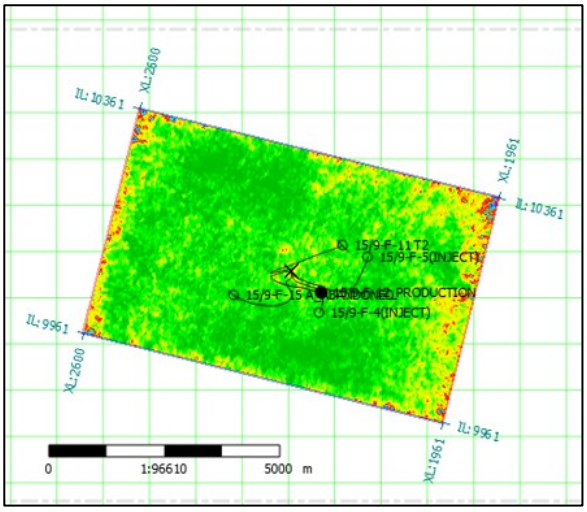

Fig. 2. NRMS difference (calculated within the interval of 2200 ms-2300 ms)

Table 1. NRMS Value Categories between Baseline and Monitor Data (Lumley, 1996)

NRMS	Comment
<0.1	Outstanding repeatability
<0.2	Excellent repeatability
0.2-0.4	Very good repeatability
0.4-0.6	Reasonable repeatability
0.6-0.8	Poor repeatability
0.8-1.2	Highly nonrepeatable
1.40	Equivalent to two random data sets
2.00	Data sets are identical, but polarity is reversed.

3.4 4D Seismic Inversion

In this study, 4D seismic inversion is employed with the objective of predicting changes in acoustic properties between baseline and monitor datasets acquired over the same field at different times (Rosa et al., 2020). In this case, water injection activities and reservoir production are considered the primary factors causing differences between the baseline and monitor datasets. In previous studies, such as the CO_2 sequestration project at the Sleipner field, the growth of the CO_2 plume was monitored using this method. Seismic analysis results provided insights into reservoir compartmentalization and the characterization of subsurface fluid flow behavior (Lumley, 2001).

In the present study, 4D inversion is performed using a model-based inversion approach on two seismic datasets. The 4D signal is obtained by subtracting the monitor seismic acoustic impedance from the baseline seismic acoustic impedance, which can be expressed by the following equation (Danaei et al., 2018)

$$4D_{\text{Signal}} = \text{Seismic Attr}\,{}^{2010}_{\text{Monitor}} - \text{Seismic Attr}\,{}^{2002}_{\text{Baseline}} \quad (1)$$

Model-based inversion is a process that modifies acoustic impedance values and layer thicknesses using Generalized Linear Inversion (Cooke and Schneider, 1983). The governing equation can be expressed as follows:

$$M = F(m_1, m_2, m_3, \dots, m_k)^T \quad (2)$$

$$M = F(m_1, m_2, m_3, \dots, m_k)^T \quad (3)$$

$$t_i = F(m_1, m_2, m_3, \dots, m_n), i = 1,2, \dots, n \quad (4)$$

$$\mathrm{F}(M) = \mathrm{F}(M_o) + \frac{\partial F(M_0)}{\partial M}\Delta M \quad (5)$$

Equation (2) represents an n-dimensional vector of the acoustic impedance (AI) model, while T in Equation (3) denotes an n-dimensional vector of the observed data. These two quantities are subsequently linked through Equations (4) and (5), where F is a function that describes the relationship between the AI model and the observed data.

Here, M_o represents the initial acoustic impedance model, ΔM denotes the perturbation or change in the model parameters, F(M) corresponds to the observed data in the form of seismic traces, $\mathrm{F}(M_o)$ represents the synthetic seismogram, and $\frac{\partial F\,(M_0)}{\partial M}$ denotes the sensitivity matrix or the response of the data to changes in the model parameters (Russell, 1988).

The error vector between the observed data and the synthetic data is defined in Equation (6) and can be reformulated as Equation (7) as follows:

$$\Delta F = F(M) - F(M_o) \quad (6)$$

$$\Delta F = G\Delta M \quad (7)$$

$$\Delta M = G^{-1}\Delta F \quad (8)$$

In Equation (8), **G** represents the derivative (Jacobian) matrix with n rows and k columns. The error exhibits a decreasing trend with successive iterations, and the iteration process continues until the error falls below a predefined threshold. Under this condition, the solution to the equation can be expressed as shown in Equation (9).

This equation represents an overdetermined case, in which the number of observations typically exceeds the number of model parameters. As a result, the inverse of matrix **G** cannot be directly computed. To address this issue, the solution can be formulated as shown in the following equation:

$$\Delta M = (G^T G)^{-1} G^1 \Delta F \quad (9)$$

The principle of model-based inversion is based on an iterative comparison between an initial model and the available seismic data. It should be noted that the results of model-based inversion are highly dependent on the wavelet used. The same seismic trace can be generated using different wavelets; therefore, this inversion approach exhibits non-uniqueness with respect to some wavelets.

4. Results and Discussion

Theoretically, acoustic impedance in a reservoir is influenced by several factors, including lithology, porosity, and fluid saturation. Among these parameters, changes in pore fluid saturation play a significant role in altering elastic properties, particularly in dynamic reservoir environments such as those affected by water injections or hydrocarbon production. Consequently, variations in acoustic impedance are commonly used as indicators of fluid substitution effects in time-lapse (4D) seismic studies.

The sensitivity of acoustic impedance to water injections has been demonstrated in previous studies. For instance, Danaei et al. (2018) conducted a qualitative 4D seismic interpretation for water injection monitoring in a

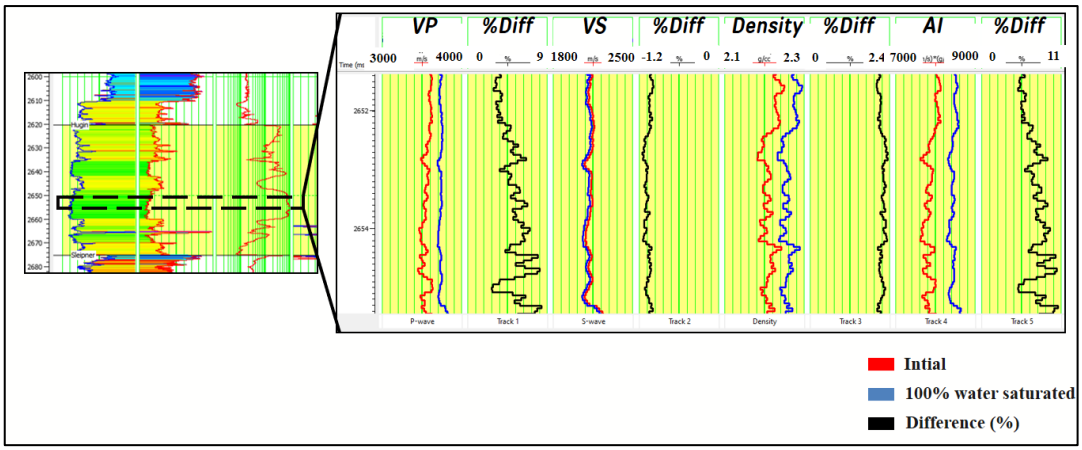

Fig. 3. Fluid Replacement Model (in situ condition replaced by water) at Hugin Interval

Southeast Asian oil field undergoing Enhanced Oil Recovery (EOR). In their study, baseline seismic data was acquired in 1995 prior to the commencement of production and injection activities, while a monitor survey was conducted in 2006 to capture reservoir changes following the initiation of water injection in 2000. By comparing inversion results from baseline and monitoring seismic datasets, the study successfully identified water movement within the reservoir. Seismic amplitude differences, along with 4D seismic attributes such as phase shifts and acoustic impedance inversion, were shown to be effective in delineating injected water distribution.

In that study, acoustic impedance models for the baseline and monitor datasets were inverted separately using a model-driven inversion approach, with the initial model derived from the baseline seismic volume. The inversion results revealed an increase in acoustic impedance around injection wells, which was interpreted as the replacement of oil by injected water within the reservoir. Furthermore, the spatial distribution of the impedance changes provided insights into sweep efficiency: relatively uniform impedance increases were observed around five injectors located in structurally lower areas, while a non-uniform distribution around an injector in a structurally higher area indicated inefficient oil sweep. These findings highlight the capability of 4D seismic inversion to capture both fluid movement and reservoir heterogeneity.

In the present study, a similar physical basis underpins the interpretation of acoustic impedance changes. **Figure 4** presents a rock physics–based modeling of the F-4 injection well data, designed to simulate reservoir conditions under the assumption of complete fluid substitution by water. This modeling was performed within the Middle Zone of the

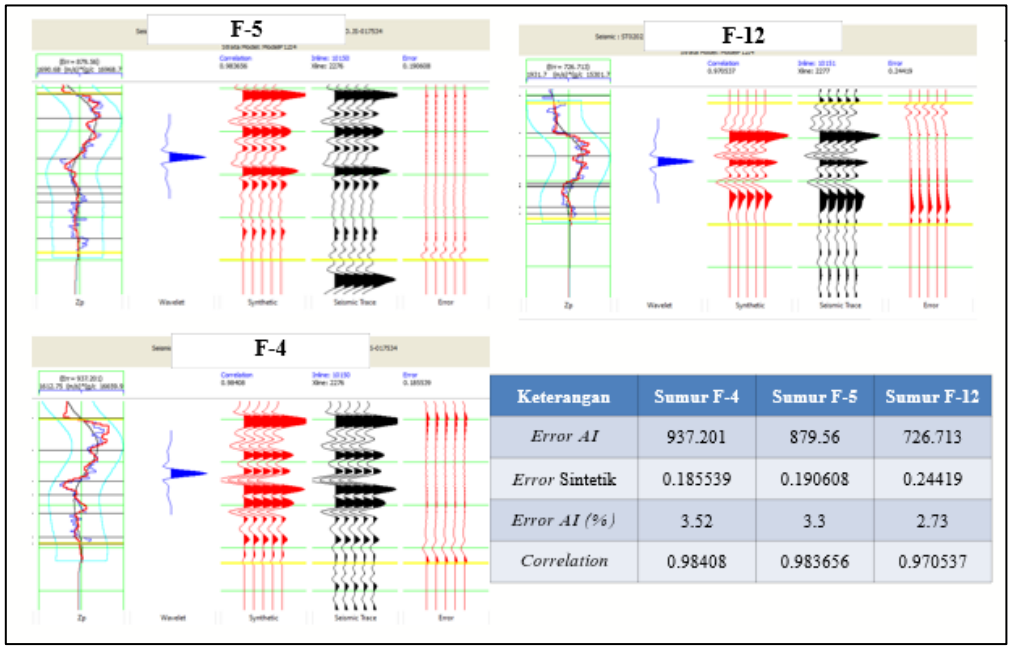

Keterangan	Sumur F-4	Sumur F-5	Sumur F-12
Error AI	937.201	879.56	726.713
Error Sintetik	0.185539	0.190608	0.24419
Error AI (%)	3.52	3.3	2.73
Correlation	0.98408	0.983656	0.970537

Fig. 4. Inversion Analysis (Baseline)

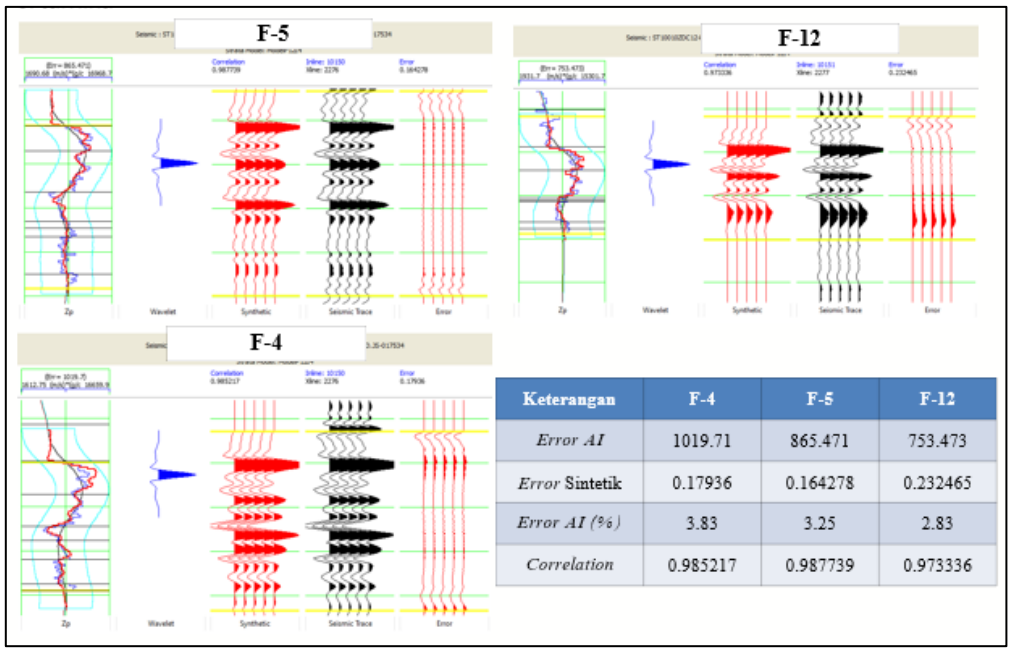

Keterangan	F-4	F-5	F-12
Error AI	1019.71	865.471	753.473
Error Sintetik	0.17936	0.164278	0.232465
Error AI (%)	3.83	3.25	2.83
Correlation	0.985217	0.987739	0.973336

Fig. 5. Inversion Analysis (Monitor)

Hugin Formation, at depths ranging from 10,900 to 10,950 ft measured depth (MD) from the surface. The selected interval is characterized by relatively homogeneous lithology, dominated by clean sandstone, thereby minimizing lithological variability and allowing the elastic response to be primarily attributed to changes in fluid properties.

The initial reservoir parameters were derived from in-situ fluid conditions, based on water saturation logs and oil fill-up data. Fluid properties were adopted from established reference values, with bulk modulus values of 2.38 GPa for water and 1 GPa for oil, and corresponding fluid densities of 1.09 g/cc and 0.75 g/cc, respectively. Matrix density was calculated using density and porosity logs, while the mineral composition was estimated from volume of shale (VSH) logs, with the non-shale fraction assumed to be composed predominantly of quartz. These assumptions are consistent with the geological setting of the Hugin Formation and provide a realistic framework for forward elastic modeling.

In **Figure 3**, the red curve shows Vp (P wave velocity), Vs (shear wave velocity), and bulk density values under initial reservoir conditions, while the blue curve shows these values after a complete replacement with water using Gassmann Fluid Substitution workflow. A detailed tutorial on how to perform fluid substitution using Gassmann is presented by Smith et al. (2003). The black curve illustrates the percentage change between these two states. As shown, the P-wave velocity increases by about 0–9% following water replacement, while the S- wave velocity remains relatively unchanged, with a slight decrease of about 0–1.2%. For the bulk density response, there is an increase of approximately 0–2.4%, which subsequently increases the acoustic impedance by around 9% from its initial state. Using this basic modeling as a reference, it can be inferred that a positive change in acoustic impedance observed in the 4D signal may likely result from water injection effects.

5. 4D Seismic Inversion Analysis

The inversion analysis was conducted within the target zones of both the baseline and monitor datasets with the objective of achieving a good match among the well data (blue curve), the low-frequency model (black curve), and the inversion results (red curve), as illustrated in **Figure 4** and **Figure 5**. This step was performed as a quality control (QC) measure to evaluate the reliability of the inversion results. The inversion error values are also presented in the blue-colored table.

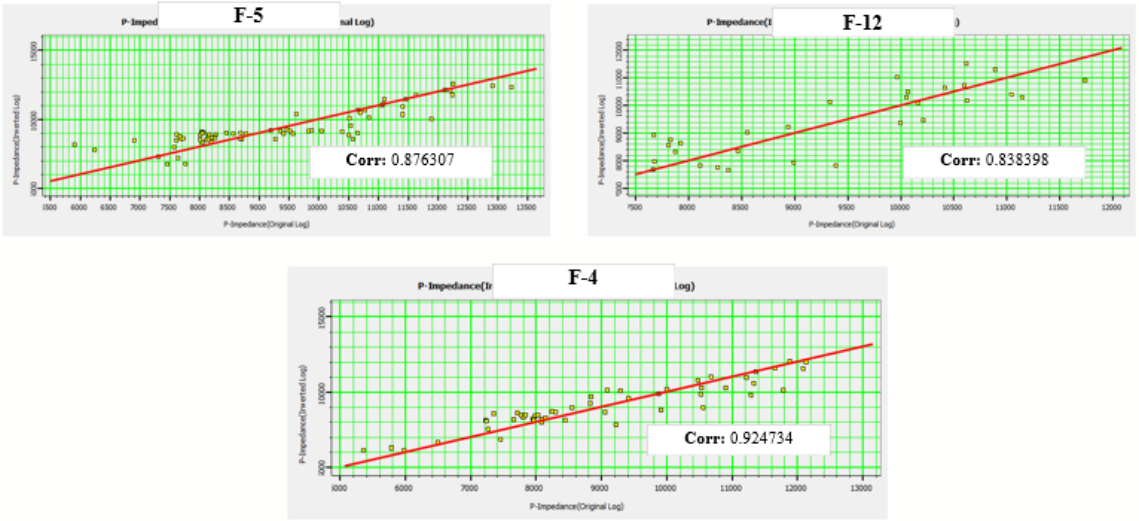

Fig. 6. P-impedance well vs Inverted (Baseline)

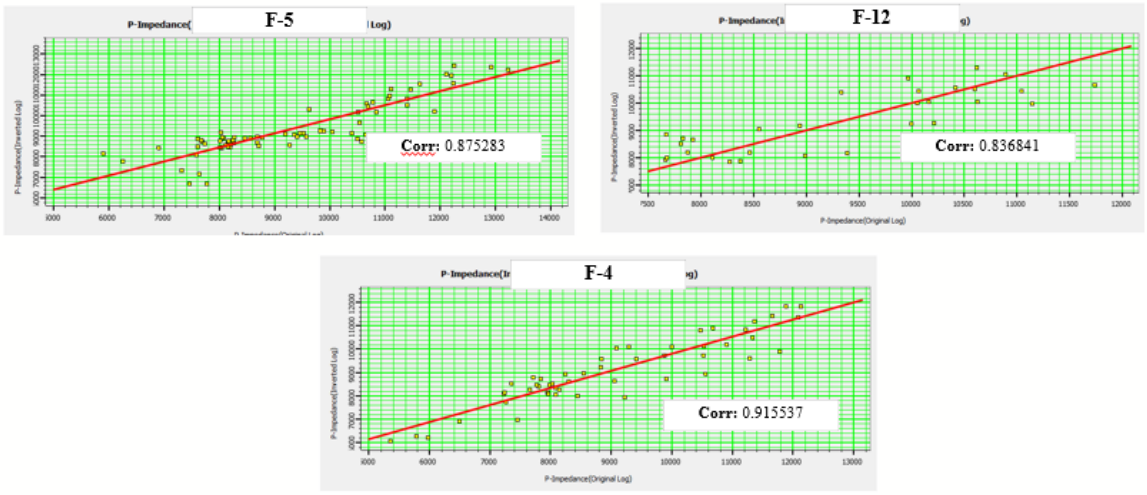

Fig. 7. P-impedance well vs Inverted (Monitor)

The inversion results can be considered satisfactory when the well data, inversion results, and low-frequency model exhibit similar trends or overlap, indicating good agreement between the inverted data and the well logs. Based on the analysis, the resulting acoustic impedance error ranges from approximately 2% to 4%.

Figure 6 illustrates the inversion correlation analysis using a crossplot between the well-derived P-impedance values and the inverted P-impedance values for the baseline seismic volume. Similarly, **Figure 7** presents the corresponding crossplot for the monitor seismic volume. These crossplot are used to quantitatively evaluate the level of agreement between the inversion results and the well log data, which serves as an independent reference for assessing inversion accuracy.

The distribution of data points in both figures shows a clear linear trend, indicating a strong positive relationship between the well P-impedance and the inverted P-impedance values. The calculated average correlation coefficient of approximately 0.8 suggests a high degree of consistency between the two datasets. This level of correlation indicates that the inversion process successfully captures the primary acoustic impedance variations observed in the well logs for both the baseline and monitor volumes.

Overall, the high correlation observed in these crossplot provides confidence in the inverted P-impedance volumes and supports their use for further quantitative analysis, including the interpretation of fluid-related changes and reservoir property variations derived from the 4D seismic inversion results.

Information on the acoustic impedance distribution for both the baseline and monitor seismic volumes, derived from time-lapse seismic inversion, is presented in **Figure 8** and **Figure 9**, with impedance values ranging from 6,770 to 12,008 (m/s)*(g/cc). Although both seismic volumes underwent simultaneous inversion using the same parameters, there are slight differences in acoustic impedance values, as indicated by the black arrows.

These differences, while relatively small in magnitude, are visually discernible in the impedance maps. For example, the area indicated by the left arrow appears yellow in the baseline seismic volume, whereas it exhibits a red coloration in the monitor volume, indicating a localized increase in acoustic impedance. A similar pattern is observed in the area marked by the right arrow, where the baseline volume shows a slightly greenish color that

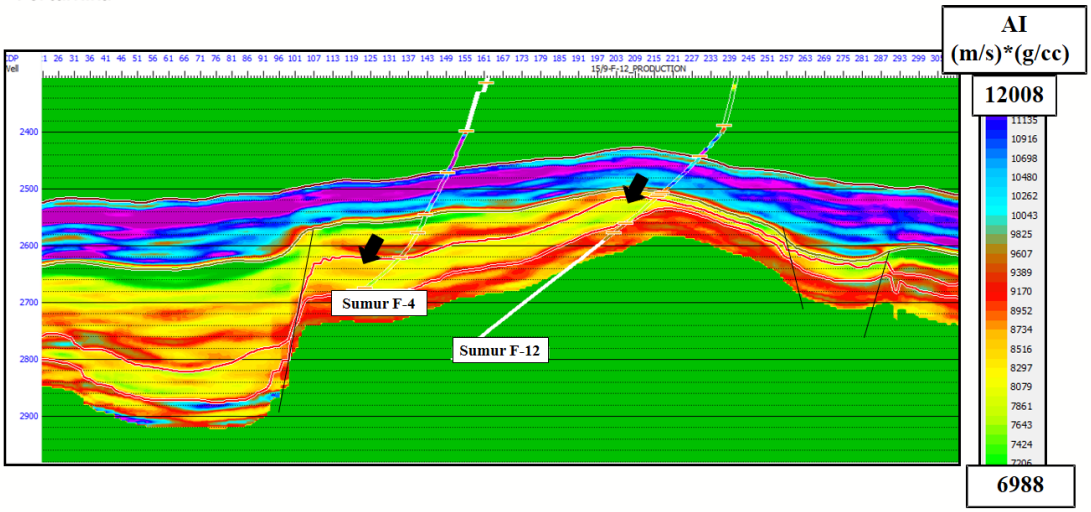

Fig. 8. Inverted Baseline

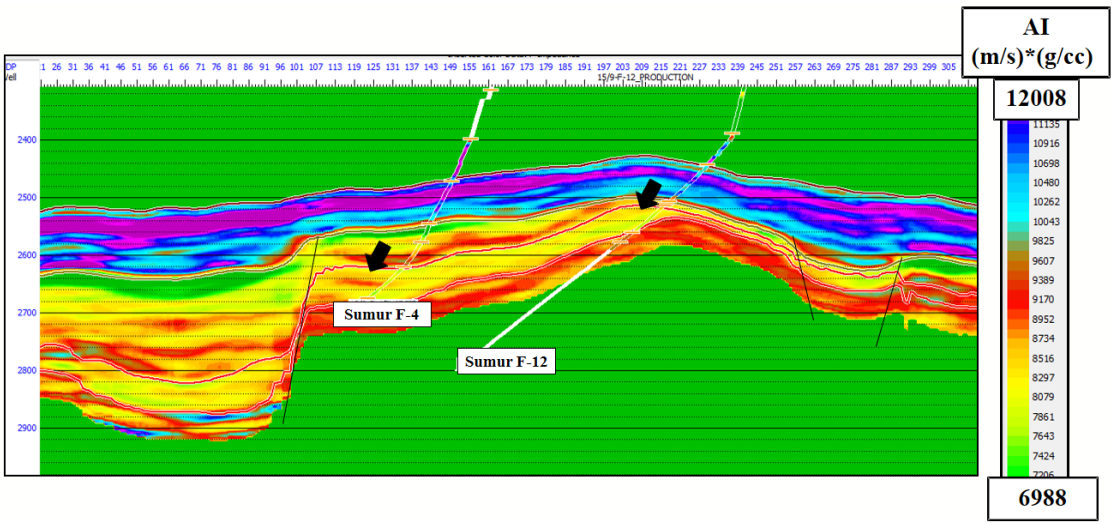

Fig. 9. Inverted Monitor

transitions to a yellowish hue in the monitor volume. Such color changes are indicative of an increase in acoustic impedance values between the baseline and monitor surveys.

The presence of these impedance increases, despite the use of consistent inversion parameters, suggests that the observed variations are not inversion artifacts but rather reflect genuine changes in reservoir properties over time. These changes are interpreted to be primarily associated with reservoir dynamic processes, particularly water injection from well F-4 and hydrocarbon production from well F-12. Water injections increase fluid saturation and, in some cases, reservoir pressure, both of which can lead to higher acoustic impedance values, while production activities may further redistribute fluids within the reservoir.

The comparison between the baseline and monitor impedance volumes demonstrates the sensitivity of the time-lapse seismic inversion to subtle reservoir changes. The observed impedance differences provide important qualitative evidence supporting the presence of injection- and production-related effects, which are further quantified and analyzed through the 4D acoustic impedance difference maps discussed in subsequent sections.

When data slicing is applied to the inverted seismic volumes, lateral variations in acoustic impedance become more clearly resolved, as highlighted by the black arrows in **Figure 10** and **Figure 11**. This slicing technique enables a focused examination of impedance changes within a specific stratigraphic interval, thereby reducing vertical averaging effects and enhancing the visibility of spatial patterns associated with reservoir dynamics.

In the vicinity of the wells, a distinct color transition can be observed from red in the baseline volume to blue in the monitor volume. This color shift signifies an increase in acoustic impedance between the two seismic surveys. Such lateral impedance changes are interpreted to reflect alterations in reservoir properties over time, primarily driven by fluid substitution processes related to water injection and hydrocarbon production activities.

If data slicing is performed, the lateral changes in acoustic impedance become more apparent, as indicated by the black arrows in **Figure 10** and **Figure 11**. In the well area, the color shifts from red in the baseline volume to blue

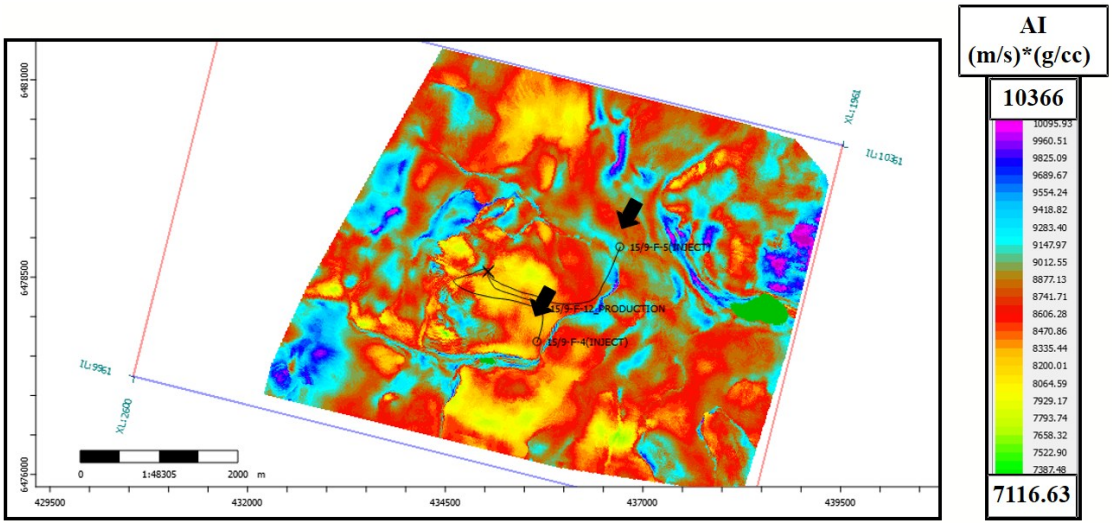

Fig. 10. Slicing Data on Inverted Baseline at Hugin interval

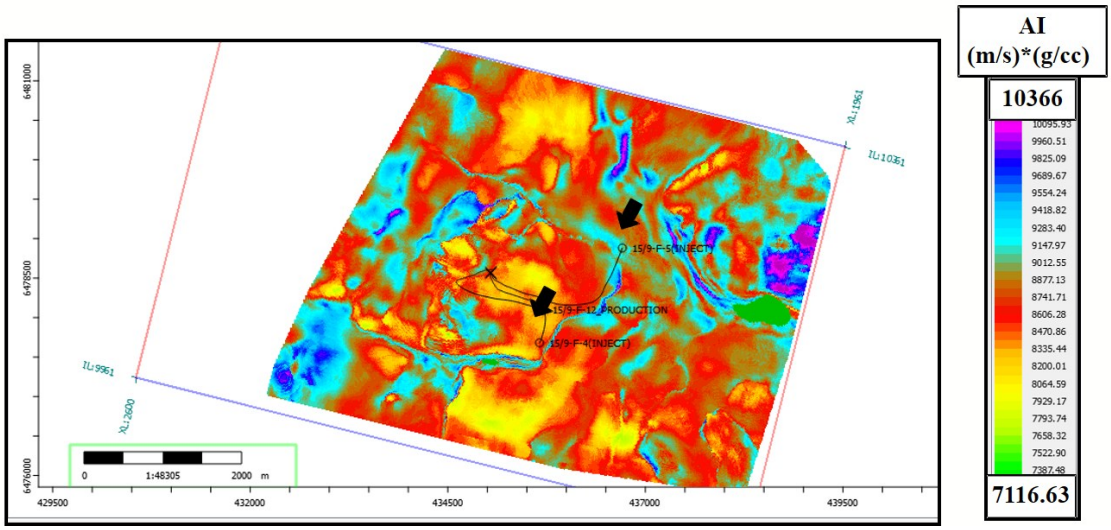

Fig. 11. Slicing Data on Inverted Monitor at Hugin Interval

in the monitor volume, indicating an increase in acoustic impedance.

6. Acoustic Impedance Difference Analysis

Figure 12 presents a map of acoustic impedance (AI) changes expressed in percentage terms, highlighting the spatial variability of impedance variations within the reservoir. As shown, the magnitude of AI changes ranges from approximately −2.64% to +2.74%, indicating both increases and decreases in acoustic impedance across the reservoir interval. This AI change map is generated by subtracting the inverted acoustic impedance values of the baseline seismic volume from those of the monitor volume, thereby isolating the time-lapse (4D) seismic response associated with changes in reservoir conditions. The resulting distribution of AI differences is further illustrated in **Figure 12** and **Figure 13**.

A prominent feature in the AI change map is the area indicated by the black arrow, which exhibits a positive change in acoustic impedance. This anomaly is interpreted as the combined effect of water injection from well F-4 and hydrocarbon production from well F-12. Well F-4 is an injection well in the Volve Field that was designed to maintain reservoir pressure, with an initial injection rate of approximately 7,500 m^3/day that stabilized at around 5,000 m^3/day by 2012. Water injections commenced in 2008, and the monitor survey acquired in 2010 captures the early response of the reservoir to this injection activity, as evidenced by an increase in acoustic impedance of up to approximately 2.74%.

To further analyze the spatial extent of these impedance changes, a slice of the AI difference volume was extracted along the top-to-base interval of the Hugin reservoir, as shown in **Figure 13**. This slice reveals the lateral distribution of acoustic impedance variations and provides clearer insight into the areal influence of injection and production processes. The results show a distinct zone of positive AI change surrounding the injection well, consistent with increased water saturation within the reservoir.

Notably, the slicing analysis indicates that the acoustic impedance changes associated with the F-4 injection well do not propagate downward. This observation suggests the presence of a sealing fault that restricts vertical fluid

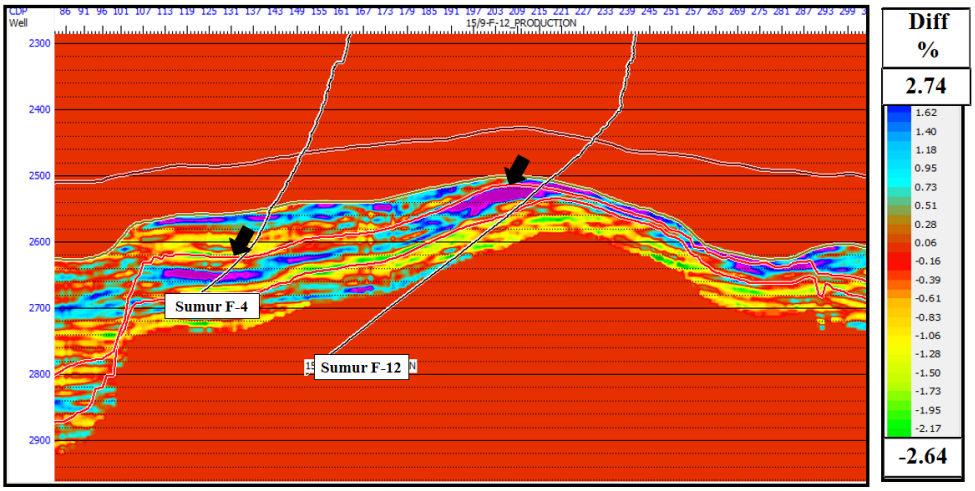

Fig. 12. Acoustic Impedance Difference between Baseline and Monitor

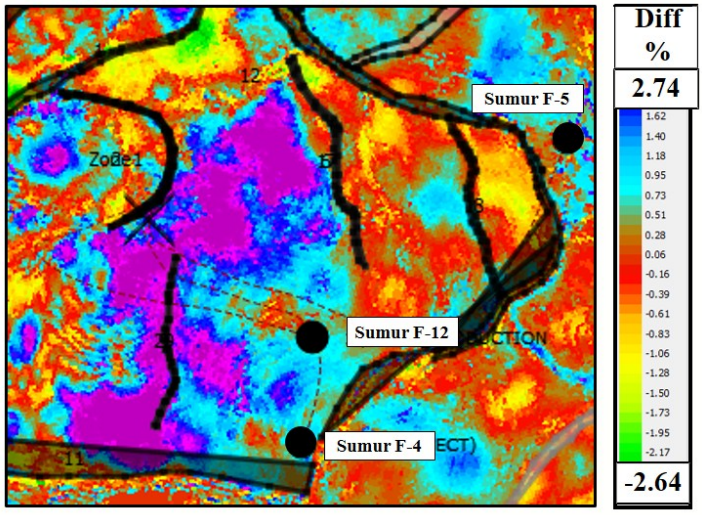

Fig. 13. Slicing Result of Acoustic Impedance Difference Volume

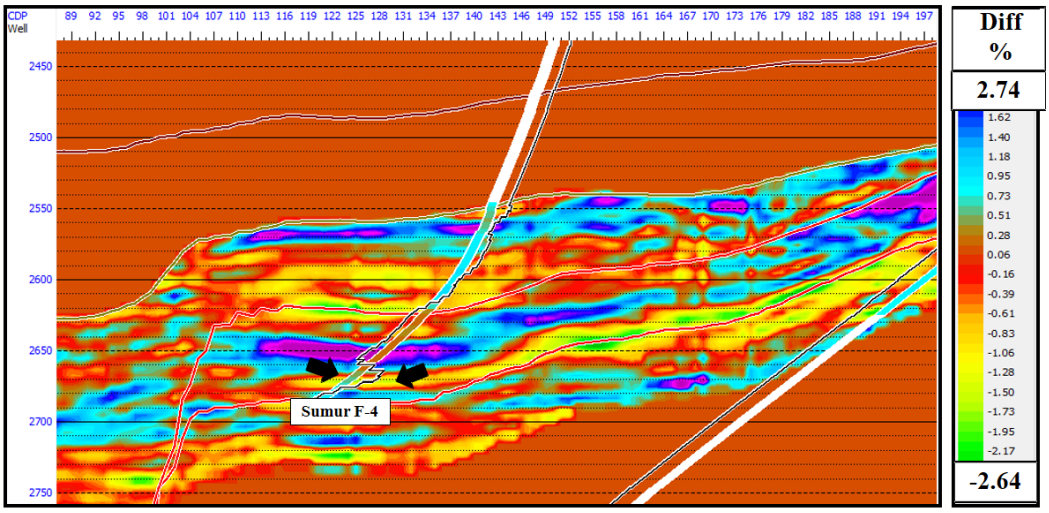

Fig. 14. Log VShale Correlation with Diff AI

movement. Instead, the injected water is preferentially directed laterally toward the F-12 production well, reflecting the compartmentalized nature of the reservoir. This interpretation is consistent with the structural framework of the field and demonstrates the capability of 4D seismic inversion to delineate fluid flow pathways and identify barriers to flow within the reservoir.

Overall, the observed spatial patterns of acoustic impedance change provide strong evidence that the detected 4D seismic response is primarily driven by reservoir dynamic processes, particularly water injection and hydrocarbon production. These results underscore the value of time-lapse seismic inversion as an effective tool for monitoring reservoir behavior and improving understanding of subsurface fluid movement.

In the Hugin Formation, there is an area at the bottom that exhibits a negative difference of acoustic impedance. This can be interpreted as the Lower Hugin zone, which is known to be heavily infiltrated by shale. Consequently, this lower layer acts as a barrier to fluid movement. **Figure 14** presents the VSH log from well F-4, correlating with the area that is suspected to be unaffected by injection activities. In the image, it is evident that the region with a negative difference value has a higher shale volume compared to the upper area.

7. Conclusion

The inversion results of the two seismic volumes indicate an increase in acoustic impedance values in the monitor volume, particularly in areas near the water injection and production wells, with an increase of approximately 3%. Based on the inversion results from the baseline and monitoring seismic volumes, it is interpreted that the injection fluid moves toward the production well and continues to the northwest. However, within the Hugin Formation, the dominant fluid movement occurs in the Middle Zone, rather than the Lower Hugin Zone. This behavior is likely controlled by the increased shale content in the Lower Hugin Zone, which acts as a permeability barrier and restricts downward fluid movement.

Acknowledgements

The author would like to express deep gratitude to Geosoftware and Equinor, whose generosity in providing essential data and access to advanced software made this research possible.

Data and Material Availability

Data and material associated with this study are available and can be accessed from https://co2datashare.org/.

References

Cooke, D.A. and Schneider, W.A., 1983. Generalized linear inversion of reflection seismic data. Geophysics, 48(6), pp.665–676. https://doi.org/10.1190/1.1441497

Danaei, S., Hermana, M. and Ghosh, D.P., 2018. 4D seismic qualitative interpretation for water injection monitoring: Case study in Southeast Asia. In: Offshore Technology Conference Asia, March 2018. OTC. https://doi.org/10.4043/28505-MS

Lumley, D., 1996. 4D seismic reservoir monitoring. Course book.

Lumley, D.E., 2001. Time-lapse seismic reservoir monitoring. Geophysics, 66(1), pp.50–53. https://doi.org/10.1190/1.1444921

Rosa, D.R., Santos, J.M., Souza, R.M., Grana, D., Schiozer, D.J., Davolio, A. and Wang, Y., 2020. Comparing different approaches of time-lapse seismic inversion. Journal of Geophysics and Engineering, 17(6), pp.929–939. https://doi.org/10.1093/jge/gxaa053

Russell, B.H., 1988. Introduction to seismic inversion methods. Tulsa, OK: Society of Exploration Geophysicists. https://doi.org/10.1190/1.9781560802303

Sastra, M.M., 2023. Karakteristik reservoir hidrokarbon silisiklastik: Studi kasus Formasi Hugin, North Sea. UNISTEK, 10(1), pp.13–24. https://doi.org/10.33592/unistek.v10i1.3299

Sen, S. and Ganguli, S.S., 2019. Estimation of pore pressure and fracture gradient in the Volve Field, Norwegian North Sea. In: SPE Oil and Gas India Conference and Exhibition, April 2019. SPE. https://doi.org/10.2118/194578-MS

Smith, T.M., Sondergeld, C.H. and Rai, C.S., 2003. Tutorial Gassmann fluid substitutions. Geophysics, 68(2), pp.430–440. https://doi.org/10.1190/1.1567211

Szydlik, T., Smith, P., Way, S., Aamodt, L. and Friedrich, C., 2007. 3D PP/PS prestack depth migration on the Volve Field. First Break, 25, pp.43–47. https://doi.org/10.3997/1365-2397.25.1106.27412